Frontiers in Bioscience Landmark

Front. Biosci. (Landmark Ed) **2026**; 31(11): 56630
https://doi.org/10.31083/FBL56630

Original Research

TRAF5 in Osteoclastogenesis and Titanium Particle-Induced Osteolysis: Functional Involvement of TNFRSF13C

Hui-Min Liu[1], Ji-Huan Li[1], Hao Zheng[1], Yong-Yun Lian[1,*]

[1]Department of Orthopaedic Surgery, The Fourth Affiliated Hospital of Harbin Medical University, 150001 Harbin, Heilongjiang, China
*Correspondence: liandadong@163.com (Yong-Yun Lian)
Academic Editor: Elisa Belluzzi
Submitted: 2 August 2026 Revised: 29 September 2026 Accepted: 30 September 2026 Published: 20 November 2026

Abstract

Background: Wear particle-induced osteolysis is a major cause of aseptic implant loosening, but the molecular regulators that connect inflammatory signaling to pathological osteoclastogenesis remain incompletely defined. This study investigated the role of tumor necrosis factor receptor-associated factor 5 (TRAF5) in titanium particle-induced osteolysis and its relationship with tumor necrosis factor receptor superfamily member 13C (TNFRSF13C). **Methods:** Public bulk transcriptomic (GSE234863) and single-cell RNA sequencing (GSE169396) datasets were analyzed to identify and prioritize candidate regulators. Protein association databases and AlphaFold3 modeling were used to generate interaction hypotheses. TRAF5 function was examined in RAW264.7 cells and primary osteoclast cultures using lentiviral overexpression and short hairpin RNA knockdown. Gene and protein expression, transcriptomic changes, and osteoclast formation were assessed by reverse transcription quantitative polymerase chain reaction, Western blotting, RNA sequencing, and tartrate-resistant acid phosphatase (TRAP) staining. A murine calvarial model was used to evaluate local TRAF5 silencing *in vivo*. **Results:** Integrated analyses identified TRAF5 as a titanium particle-associated and RANK-linked candidate. In the GSE169396 dataset, TRAF5 and TNFRSF13C were detected in a predominantly B-cell-associated cluster. In primary osteoclast cultures, TRAF5 overexpression increased the formation of TRAP-positive multinucleated cells and elevated Fos proto-oncogene, AP-1 transcription factor subunit (c-Fos)/nuclear factor of activated T cells 1 (NFATc1) protein levels, whereas TRAF5 knockdown reduced c-FOS protein levels in primary cultures and decreased both c-FOS and NFATc1 protein levels in RAW264.7 cells. RNA sequencing linked TRAF5 overexpression to oxidative phosphorylation-related gene sets. TNFRSF13C silencing attenuated, but did not abolish, TRAF5-associated increases in c-FOS/NFATc1 expression, while reducing osteoclast formation. *In vivo*, local administration of TRAF5-targeting shRNA lentivirus was associated with higher bone volume/total volume (BV/TV) and lower total porosity than titanium particle treatment alone. In an independent calvarial cohort, this treatment reduced the mRNA expression of TRAF5, TNFRSF13C, and *Rela* (encoding NF-κB p65). However, the *in vivo* studies were limited by the inclusion of only three mice per group, the absence of a titanium particle plus non-targeting shRNA lentivirus control, and the lack of assessment of local TRAF5 protein expression. **Conclusions:** These findings support a positive regulatory role for TRAF5 in osteoclast differentiation and suggest that TNFRSF13C is functionally involved in TRAF5-associated osteoclastogenic responses. Exploratory *in vivo* findings further suggest that TRAF5 may contribute to titanium particle-induced calvarial osteolysis, providing a basis for further mechanistic investigation and evaluation of the potential utility of targeting TRAF5-related signaling.

Keywords: periprosthetic osteolysis; osteoclastogenesis; TRAF5; TNFRSF13C; NF-κB; titanium wear particles; bone resorption

1. Introduction

Periprosthetic osteolysis and aseptic loosening remain major causes of long-term failure after total joint arthroplasty [1,2]. Wear particles, including titanium particles released from implant surfaces, disturb the balance between bone formation and resorption [3,4,5]. Macrophages and other cells recognize these particles and produce inflammatory mediators, including tumor necrosis factor-α, interleukin (IL)-1β, IL-6, and IL-17 [6,7]. These signals promote osteoclastogenesis through the receptor activator of nuclear factor kappa B ligand (RANKL)/receptor activator of nuclear factor kappa B (RANK)/osteoprotegerin axis and can suppress osteoblast differentiation through pathways that include Wnt/β-catenin signaling [8,9,10,11]. Programmed cell death pathways may further sustain tissue injury in the periprosthetic microenvironment [2,12]. While anti-resorptive and anti-RANKL approaches target important downstream events, upstream regulators of particle-induced inflammatory bone loss remain of interest [6,13].

Tumor necrosis factor receptor-associated factors (TRAFs) are adaptor proteins and E3 ubiquitin ligases that couple cell-surface receptors to intracellular signaling [14,15,16,17]. TRAF6 is the canonical adaptor downstream of RANK, while TRAF5 has also been implicated in RANKL- and tumor necrosis factor-α-induced osteoclastogenesis [18]. However, the specific contribution of TRAF5 to wear particle-induced osteolysis has yet to be established. Our preliminary computational intersection of titanium particle-responsive genes and RANK-associated proteins prioritized TRAF5, providing a rationale for inves-

Copyright: © 2026 The Author(s). Published by IMR Press.
This is an open access article under the CC BY 4.0 license.

Publisher's Note: IMR Press stays neutral with regard to jurisdictional claims in published maps and institutional affiliations.

tigating its functional role in wear particle-induced osteolysis.

TNFRSF13C, also known as B-cell activating factor receptor, can recruit TRAF proteins and regulate nuclear factor kappa B (NF-κB) and mitogen-activated protein kinase signaling [19,20,21]. Although TNFRSF13C has been most thoroughly characterized in B-cell biology, its expression in other immune populations and its association with inflammatory disease suggest it may have broader functions [22,23,24]. Whether it participates in TRAF5-associated osteoclast differentiation remains unknown. We therefore integrated public bulk and single-cell transcriptomic analyses with gain- and loss-of-function experiments and with a murine calvarial model to determine whether TRAF5 acts as a regulator of wear particle-induced osteoclastogenesis, and whether TNFRSF13C functionally contributes to these effects.

2. Materials and Methods

2.1 Public Transcriptomic and Network Analyses

The GSE234863 bulk transcriptomic dataset and the GSE169396 single-cell RNA-sequencing dataset were obtained from the Gene Expression Omnibus (GEO) (https://www.ncbi.nlm.nih.gov/geo/). Differential expression analysis of FPKM- or TPM-normalized data was performed with limma version 3.58.1 (Gordon Smyth and contributors; Walter and Eliza Hall Institute of Medical Research, Melbourne, Australia; https://bioconductor.org/packages/limma/) using $|\log_2 FC| \geq 0.5$ and an unadjusted p-value < 0.05. For the intersection analysis, 777 downregulated genes meeting $\log_2 FC \leq -1$ and an unadjusted p-value < 0.05 were selected. Gene set enrichment analysis (GSEA) was conducted with clusterProfiler version 4.10.1 (Guangchuang Yu and contributors; Southern Medical University, Guangzhou, China; https://bioconductor.org/packages/clusterProfiler/). Protein association networks were assembled from BioGRID (https://thebiogrid.org/) and STRING (https://string-db.org/), and a STRING confidence threshold of at least 0.7 was applied. Single-cell analysis was performed with Seurat version 5.0.3 (Satija Lab, New York Genome Center, New York, NY, USA) at a clustering resolution of 0.5. Cluster marker genes were ranked by fold change and p-value, with the top 30 marker genes for each cluster used for cell-type annotation. Cell-type annotations for clusters 0–18 and the top 30 marker genes for each cluster are provided in **Supplementary Tables 1,2**, respectively.

2.2 Structural Modeling

AlphaFold3 (AlphaFold Server, AlphaFold-beta-20231127; accessed November 7, 2024; Google DeepMind and Isomorphic Labs, London, UK) was used to model a putative complex between RANK and TRAF5, and predicted aligned error (PAE) matrices were inspected to assess model confidence. The model was used to evaluate structural compatibility and to generate a testable interaction hypothesis, but was not interpreted as a measurement of binding affinity or as experimental confirmation of a physical interaction.

2.3 Titanium Particle Preparation

Commercial titanium powder (Thermo Scientific Chemicals, Waltham, MA, USA; catalog no. 042624.36; CAS 7440-32-6) was acid-washed, autoclave-sterilized, and processed to remove endotoxin. Endotoxin levels were <0.05 EU/mL according to a Limulus amebocyte lysate assay (Beyotime Biotechnology, Shanghai, China; catalog no. C0266BS). For *in vivo* administration, particles were suspended in sterile phosphate-buffered saline (Biosharp, Beijing, China; catalog no. BL601A) at a working concentration of 0.3 g/mL and sonicated before use. An aliquot of 100 µL, corresponding to 30 mg of titanium particles, was administered per mouse.

2.4 Animals, Ethics, and Welfare

Male C57BL/6J mice aged 6–10 weeks and weighing 20–25 g were purchased from Liaoning Changsheng Biotechnology Co., Ltd. The *in vivo* calvarial experiment included the following groups (n = 3 mice per group): control, titanium-particle, and titanium-particle plus TRAF5-targeting shRNA lentivirus. Each point in the quantitative analyses represents one mouse. Mice were housed (n = 5 per cage) under the following conditions: 22 ± 2 °C, 50–60% humidity, a 12-hour light/dark cycle, and free access to food and water. The animals were acclimatized for at least 7 days and then allocated to groups using a random-number table.

The animal procedures were reviewed and approved by the Institutional Animal Care and Use Committee of the Fourth Affiliated Hospital of Harbin Medical University (approval no. 2025-DWSYLLCZ-142). Animal experimentation was conducted in accordance with applicable national guidelines and the ARRIVE reporting recommendations.

2.5 Mouse Calvarial Osteolysis Model and Local Gene Delivery

Mice were anesthetized with isoflurane (4–5% for induction, 1.5–2.5% for maintenance, for a total anesthesia duration of 30 min), and a midline scalp incision was made under sterile conditions. A superficial 0.5–0.8 mm window was created in the avascular parietal bone without penetrating the inner cortical plate or dura. A 100 µL aliquot of the 0.3 g/mL titanium-particle suspension, containing 30 mg of titanium particles, was delivered into the window. The site was then sealed with a sterile gelatin sponge (EpiZyme, Shanghai, China; catalog no. OT103) before layered closure. Postoperative analgesia was provided according to institutional guidelines.

For local TRAF5 silencing, recombinant lentivirus encoding TRAF5-targeting short hairpin RNA was prepared

at 10^8 transducing units/mL. Under isoflurane anesthesia, 20–30 µL was injected into the subperiosteal space at the particle implantation site on days 0, 3, 7, and 10. The needle was retained for 30 seconds before withdrawal. The *in vivo* comparison was made using control, titanium-particle, and titanium-particle plus TRAF5-targeting shRNA lentivirus groups (n = 3 mice per group). An independent validation cohort comprising the control, titanium-particle, and titanium-particle plus TRAF5-targeting shRNA lentivirus groups (n = 3 mice per group) was used to assess calvarial expression of TRAF5, TNFRSF13C, and *Rela* mRNA by reverse transcription quantitative polymerase chain reaction (RT-qPCR). Calvarial tissues were collected on day 14 after model induction.

At the experimental endpoint, mice were deeply anesthetized with 4% isoflurane. The depth of anesthesia was confirmed by loss of consciousness and absence of the toe-pinch reflex, after which trained personnel performed cervical dislocation before tissue collection.

2.6 Isolation and Differentiation of Bone Marrow-Derived Macrophages

Bone marrow-derived macrophages (BMDMs) were isolated from the femurs and tibias of 8–10-week-old mice. Marrow was flushed with ice-cold phosphate-buffered saline (Biosharp, Beijing, China; catalog no. BL601A) containing 1% fetal bovine serum (LONSERA, Suzhou, China; catalog no. S711-001S), filtered through a 70-µm mesh, treated with ACK lysis buffer (Thermo Fisher Scientific, Waltham, MA, USA; catalog no. A1049201) for 1–3 minutes, and then centrifuged at 300 ×g for 5 minutes at 4 °C. Cells were cultured in α-minimal essential medium (Thermo Fisher Scientific, Waltham, MA, USA; catalog no. 12571063) containing 10% fetal bovine serum, 1% penicillin-streptomycin (Gibco, Grand Island, NY, USA; catalog no. 15140-122), and 20–50 ng/mL of recombinant murine macrophage colony-stimulating factor (MedChemExpress, Monmouth Junction, NJ, USA; catalog no. HY-P7247). After 24 h, non-adherent cells were removed, and the remaining adherent cells were expanded using macrophage colony-stimulating factor (30 ng/mL) for 3 days, with half-medium changes every 48 h. Primary cultures were maintained at 37 °C in a humidified incubator containing 5% CO_2.

For osteoclast differentiation, BMDMs were seeded at 3×10^4 cells/cm^2 and cultured for 4–6 days in α-minimal essential medium containing 10% fetal bovine serum, 1% penicillin-streptomycin, macrophage colony-stimulating factor (30 ng/mL), and RANKL (Abbkine, Wuhan, China; catalog no. PRP1114) (50–100 ng/mL). Half of the medium was replaced every 48 h. Multinucleated tartrate-resistant acid phosphatase (TRAP)-positive cells containing at least three nuclei were classified as mature osteoclasts.

2.7 RAW264.7 Cell Culture

RAW264.7 murine macrophage-like cells (Shanghai Fuheng Biotechnology, Shanghai, China; catalog no. FH0328) were maintained in Dulbecco's modified Eagle medium (Gibco, Grand Island, NY, USA; catalog no. C11965500BT) supplemented with 10% fetal bovine serum and 1% penicillin-streptomycin at 37 °C in 5% CO_2. Cells were maintained below 80% confluence and passaged at a ratio of 1:3–1:5. For osteoclastogenesis, cells were seeded at 5×10^3 cells/well in 96-well plates, or 2×10^4 cells/cm^2 in 24-well plates, and cultured in α-minimal essential medium containing RANKL (50–100 ng/mL) without exogenous macrophage colony-stimulating factor. TRAP-positive multinucleated cells were assessed after 3–5 days. RAW264.7 cells were authenticated by short tandem repeat profiling (reference profile, CVCL_0493), and confirmed to be of mouse origin by species-specific multiplex qPCR. Both primary cultures and RAW264.7 cells were tested for mycoplasma contamination and tested negative.

2.8 Genetic Manipulation

TRAF5 was overexpressed using pLVX-FLAG-TRAF5 lentivirus (Geneppl Technology Co., Ltd., Nanjing, China; custom construct) at a multiplicity of infection of 5–20 in the presence of 8 µg/mL Polybrene (Sigma, St. Louis, MO, USA; catalog no. P1501912) or using a pcDNA3.1(+)-Flag-mTraf5-T2A-EGFP2 plasmid (Geneppl Technology Co., Ltd., Nanjing, China; catalog no. PPL50126-2b). The pLVX lentiviral system was used for stable overexpression in primary BMDM-derived osteoclast cultures, with the corresponding empty pLVX vector as the negative control. The pcDNA3.1 system was used for transient transfection of RAW264.7 cells, with the corresponding empty pcDNA3.1(+) vector as the negative control. Three TRAF5-targeting short hairpin RNA constructs (PPL50126-3d, target sequence 5′-CTACTCTGGAGAACTCCAAGA-3′; PPL50126-3e, target sequence 5′-GCTACAGTGGCAAGCTCATCT-3′; and PPL50126-3f, target sequence 5′-CCTGCAGGACCACATGCTTCT-3′; Geneppl Technology Co., Ltd., Nanjing, China) and TNFRSF13C small interfering RNA (Tnfrsf13c-Mouse-416; sense, 5′-CGCUCAAAGAAGAUGCAGATT-3′; antisense, 5′-UCUGCAUCUUCUUUGAGCGTT-3′; GeneAdv, Suzhou, China) were used for TRAF5 knockdown. Lentiviral shRNA was used for sustained TRAF5 silencing in primary cultures and for local delivery *in vivo*, whereas siRNA was used for transient TNFRSF13C silencing in cell-based rescue experiments. A non-targeting siRNA (siRNA NC; sense, 5′-UUCUCCGAACGUGUCACGUTT-3′; antisense, 5′-ACGUGACACGUUCGGAGAATT-3′; GeneAdv, Suzhou, China) served as the negative control for TNFRSF13C silencing. A non-targeting shRNA lentivirus obtained from Geneppl Technology Co., Ltd. (Nanjing, China) was used as the shNC control in cell-based TRAF5

knockdown experiments. Transduced cells were enriched with 1–2 μg/mL puromycin (KeyGEN BioTECH, Nanjing, China; catalog no. KGC67046-1).

2.9 Tartrate-Resistant Acid Phosphatase Staining

Cells were fixed in 4% paraformaldehyde (Biosharp, Beijing, China; catalog no. BL539A; https://mall.labgic-ljk.com/detail/462358) for 15 minutes at room temperature, washed, and incubated with TRAP staining solution (Solarbio, Beijing, China; catalog no. G1492) at 37 °C for 30–60 minutes. The reaction was stopped with distilled water. Cells containing at least three nuclei and positive cytoplasmic staining were counted as osteoclasts in 5–10 randomly selected fields per well.

2.10 RNA Sequencing, RT-qPCR, and Western Blotting

RNA sequencing was performed on an Illumina NovaSeq 6000 platform (Illumina, San Diego, CA, USA) using paired-end 150-base-pair reads. Differential expression was subsequently analyzed with DESeq2 version 1.42.1 (Michael I. Love, Wolfgang Huber, and Simon Anders; European Molecular Biology Laboratory, Heidelberg, Germany). RNA sequencing (RNA-seq) samples comprised vector-control and TRAF5-overexpressing RAW264.7 cells (n = 3 per group). Following mRNA enrichment and cDNA library preparation, reads were processed with fastp to remove adapters and low-quality reads, aligned to the mouse mm10 reference genome using HISAT2, and quantified using featureCounts. RNA-seq data analysis was performed using the Majorbio Cloud platform (Shanghai Majorbio Bio-pharm Technology Co., Ltd., Shanghai, China).

Total RNA was isolated with an RNA extraction kit reagent (Vazyme, Nanjing, China; catalog no. RC102-01), and complementary DNA was synthesized from 1 μg of RNA using HiFiScript cDNA Synthesis Kit (Cowin Biotech, Taizhou, China; catalog no. cW2569). RT-qPCR was performed with SYBR Green Master Mix (GLPBIO, Montclair, CA, USA; catalog no. GK10002). The RT-qPCR cycling program comprised 95 °C for 2 min, followed by 40 cycles of 95 °C for 12 s and 60 °C for 30 s, with a melting curve from 65–95 °C in 0.5 °C increments. Relative expression was calculated using the $2^{-\Delta\Delta Ct}$ method, with β-actin as the internal control. Primer sequences are provided in Table 1. For the independent calvarial cohort, each mouse was analyzed as one biological replicate (n = 3 per group), and the mRNA expression level of TRAF5, TNFRSF13C, and *Rela* was normalized to β-actin.

Protein was extracted from cells in RIPA buffer (Leagene, Beijing, China; catalog no. PS0013) containing protease and phosphatase inhibitors (Biosharp, Beijing, China; catalog no. BL615A). Protein concentration was measured by BCA assay (Beyotime Biotechnology, Shanghai, China; catalog no. P0010). Samples containing 20–30 μg of protein were separated by 10–12% SDS-PAGE, transferred to PVDF membranes (LABSELECT, Beijing, China; catalog no. TM-NC-R-22), and blocked with 5% non-fat milk or bovine serum albumin in TBST for 1 h. Membranes were incubated overnight at 4 °C with antibodies against TRAF5 (Affinity Biosciences, Liyang, China; catalog no. DF12779; dilution 1:1000), c-FOS (HUABIO, Hangzhou, China; catalog no. ET1701-95; dilution 1:500), NFATc1 (ProMab, Changsha, China; catalog no. P31358; dilution 1:1000), TNFRSF13C (ProMab, Changsha, China; catalog no. P05098; dilution 1:1000), and β-actin (HUABIO, Hangzhou, China; catalog no. HA722023; dilution 1:10,000). This was followed by incubation with horseradish peroxidase-conjugated secondary antibodies (anti-rabbit/anti-mouse IgG; Beyotime, Shanghai, China; catalog nos. A0208 and A0216, respectively; dilution 1:2000) for 1 h. Bands were detected by enhanced chemiluminescence (Xinhai Gene, Harbin, China; catalog no. M2301) and quantified with ImageJ version 1.46r (Wayne Rasband, National Institutes of Health, Bethesda, MD, USA). Raw, uncropped Western blots are available from the corresponding author upon reasonable request.

2.11 Histology, Micro-Computed Tomography, and Statistical Analysis

Calvarial specimens were evaluated by hematoxylin and eosin staining, TRAP staining, and micro-computed tomography (SkyScan 1275 micro-CT scanner; Bruker microCT, Kontich, Belgium; source voltage, 46 kV; source current, 75 μA; rotation step, 0.2°; image pixel size, 10 μm; no filter). Bone volume fraction (BV/TV) and total porosity were quantified using CTAn version 1.20.8.0 (Bruker microCT). A rectangular region of interest centered on the parietal-bone particle-application site was analyzed using a grayscale segmentation threshold of 65–255.

Quantitative data are presented as the mean ± standard deviation. Cell-based experiments were performed at least three times independently. Animal experiments included three mice per group, with each mouse representing one biological replicate. Normality was assessed with the Shapiro-Wilk test and homogeneity of variance with Levene's test. Normally distributed data with equal variances were compared using an unpaired Student's *t*-test for two groups, or one-way analysis of variance with Tukey's post hoc test for multiple groups. The Mann-Whitney U test or Kruskal-Wallis test with Dunn's post hoc test and Bonferroni adjustment for multiple comparisons was used when parametric assumptions were not met. A two-sided *p*-value < 0.05 was considered statistically significant. Statistical analyses were performed using GraphPad Prism version 10.4.1 (GraphPad Software, Boston, MA, USA) and R version 4.2.0 (R Foundation for Statistical Computing, Vienna, Austria). The three-group calvarial RT-qPCR data were analyzed by ordinary one-way analysis of variance, followed by Tukey's multiple-comparisons test.

Table 1. Primer sequences used in this study.

Primer	Sequence (5′-3′)
TRAF5 Forward primer	CACTCCGTGCTTCACAACC
TRAF5 Reverse primer	GCAGCTCTCGTTAGGGCAG
TNFRSF13C Forward primer	GGTGGGTCTAGTGAGTCTGGT
TNFRSF13C Reverse primer	TTCTGAGGAGGGTACAAAGAC
IKBKB Forward primer	GCAGACTGACATTGTGGACCTG
IKBKB Reverse primer	ATCTCCTGGCTGTCACCTTCTG
Rela Forward primer	TCCTGTTCGAGTCTCCATGCAG
Rela Reverse primer	GGTCTCATAGGTCCTTTTGCGC
β-actin (ACTB) Forward primer	CTTCCTTCCTGGGCATGG
β-actin (ACTB) Reverse primer	GCCGCCAGACAGCACTGT

TRAF5, tumor necrosis factor receptor-associated factor 5; TNFRSF13C, tumor necrosis factor receptor superfamily member 13C; IKBKB, inhibitor of nuclear factor kappa B kinase subunit beta (IKK2); *Rela*, Rela proto-oncogene.

3. Results

3.1 Integrated Analyses Prioritize TRAF5 as a Particle-Responsive, RANK-Associated Candidate

Analysis of GSE234863 identified 1507 upregulated and 931 downregulated genes in titanium particle-treated bone tissue compared with untreated tissue (Fig. 1A,B). A RANK-centered protein association network contained several TRAF family members, including TRAF6, TRAF2, and TRAF5 (Fig. 1C,D). Intersecting these 777 downregulated genes with the RANK-associated network identified TRAF5 as the only overlapping gene (Fig. 1E), thus prioritizing this gene for further study.

AlphaFold3 generated a structurally compatible model of a putative RANK-TRAF5 complex with a localized predicted interface (Fig. 1F–I). The predicted aligned error matrix supported confidence in portions of the modeled structure (Fig. 1G). Because this analysis is computational, it supports a testable interaction hypothesis. However, it does not establish binding affinity or direct physical association.

3.2 TRAF5 and TNFRSF13C are Detected in a B-Cell-Associated Single-Cell Cluster

Single-cell analysis of human femoral-head tissue in the GSE169396 dataset identified distinct cell clusters by uniform manifold approximation and projection. TRAF5 expression was enriched in cluster 14 (Fig. 2A–C), where TNFRSF13C was also found to be expressed. Gene Ontology analysis associated this cluster with skeletal muscle-related processes and with the negative regulation of osteoblast proliferation (Fig. 2D–K). These observations place TRAF5 and TNFRSF13C in a B-cell-associated transcriptional context, but do not by themselves define a distinct pathogenic lineage. Based on the top-ranked marker genes, cluster 14 was annotated as a B-cell-associated cluster (**Supplementary Table 1**).

BioGRID- and STRING-derived networks placed TRAF5 among the proteins associated with TRAF2, TRAF6, MAP3K7, and receptor-linked signaling (**Supplementary Fig. 1A,E**). Enrichment analyses highlighted NF-κB, JNK, stress-activated mitogen-activated protein kinase, cytokine-receptor, and tumor necrosis factor signaling pathways (**Supplementary Fig. 1B–D,F–H**). The databases also revealed a network link between TRAF5 and TNFRSF13C. Together with the detection of TRAF5 and TNFRSF13C within the same single-cell cluster, this association provided a rationale for experimentally testing their functional relationship. Nevertheless, it was not viewed as providing independent biochemical validation of binding.

3.3 TRAF5 Overexpression is Associated With Oxidative Phosphorylation-Related Transcriptional Programs

RNA sequencing of TRAF5-overexpressing RAW264.7 cells identified 2310 differentially expressed genes (Fig. 3A). Gene set enrichment analysis highlighted skeletal-system development and osteoclast-proliferation terms (Fig. 3B). Mitochondrial respiratory chain components, NADH dehydrogenase activity, and oxidative phosphorylation complexes were prominent in molecular-function and cellular-component networks (Fig. 3C,D), and oxidative phosphorylation, thermogenesis, and extracellular matrix-receptor interaction were among the enriched modules (Fig. 3E). These associations suggest a potential link between TRAF5 overexpression and metabolic and structural transcriptional programs. Nevertheless, direct metabolic flux was not measured.

3.4 TRAF5 Promotes Osteoclast Differentiation in Primary Cultures

The pLVX lentiviral system induced overexpression of TRAF5 in primary osteoclast cultures, as demonstrated by increased TRAF5 mRNA and protein expression (Fig.

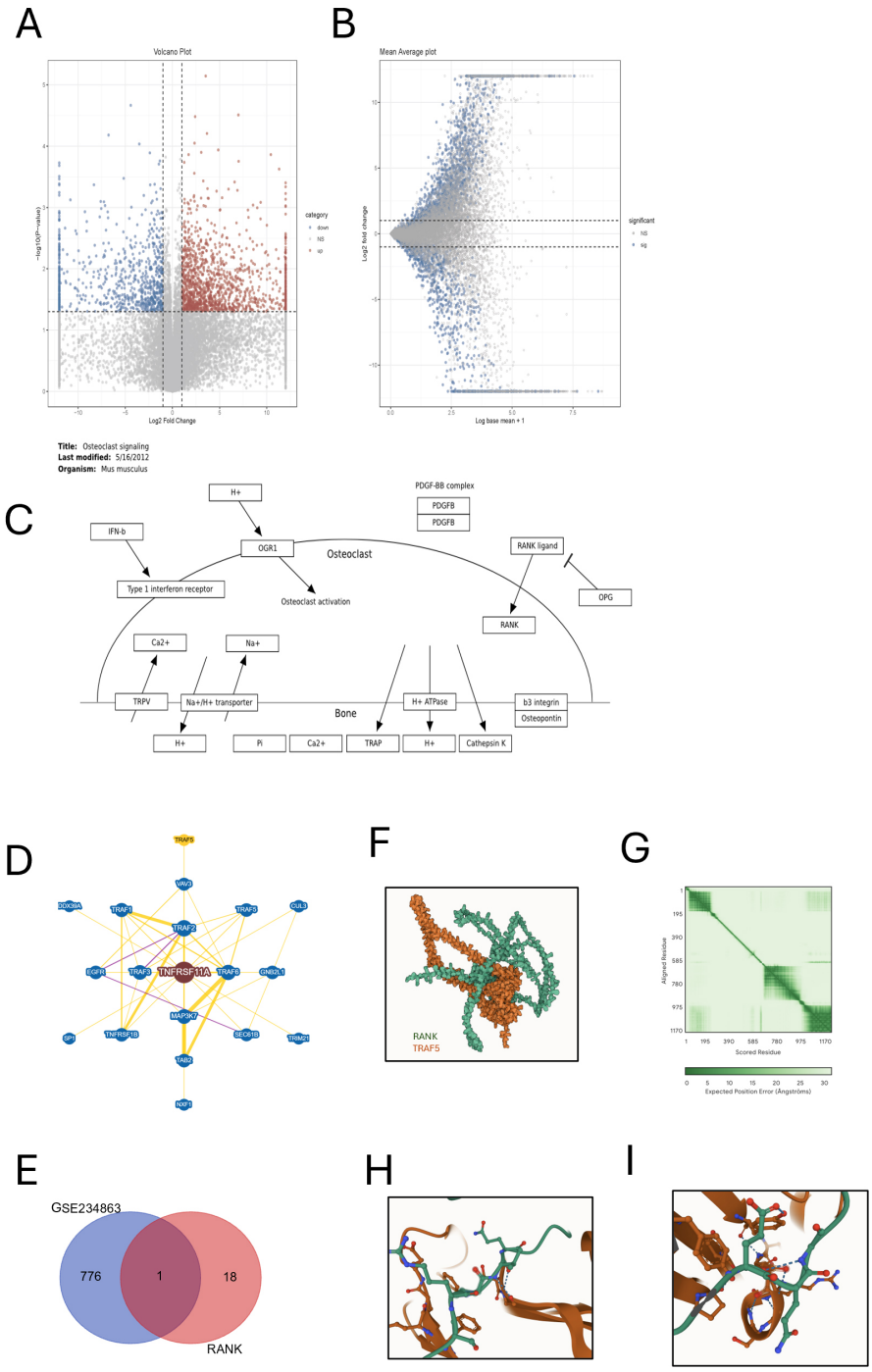


Fig. 1. Integrated analysis prioritizes TRAF5 as a particle-responsive, RANK-associated candidate. (A) Volcano plot of GSE234863 comparing titanium particle-treated and untreated samples. The x-axis shows log2 fold change and the y-axis shows the –log10 *p*-value; red, blue, and gray points denote upregulated, downregulated, and non-significant genes, respectively. (B) Mean-average plot showing fold change across expression abundance. (C) Schematic of the RANK/RANKL osteoclast signaling pathway. (D) RANK-centered protein association network containing TRAF family members and other signaling molecules. (E) Intersection of the 777 selected downregulated genes from GSE234863 and RANK-associated genes, identifying TRAF5 as the common candidate. (F) AlphaFold3 model of a putative RANK (green)-TRAF5 (orange) complex. (G) Predicted aligned error matrix. (H,I) Enlarged views of the modeled interface, with the blue dashed lines denoting predicted hydrogen bonds. The structural model is computational and does not experimentally establish binding. TRAF5, tumor necrosis factor receptor-associated factor 5; RANK, receptor activator of nuclear factor kappa B; RANKL, receptor activator of nuclear factor kappa B ligand.

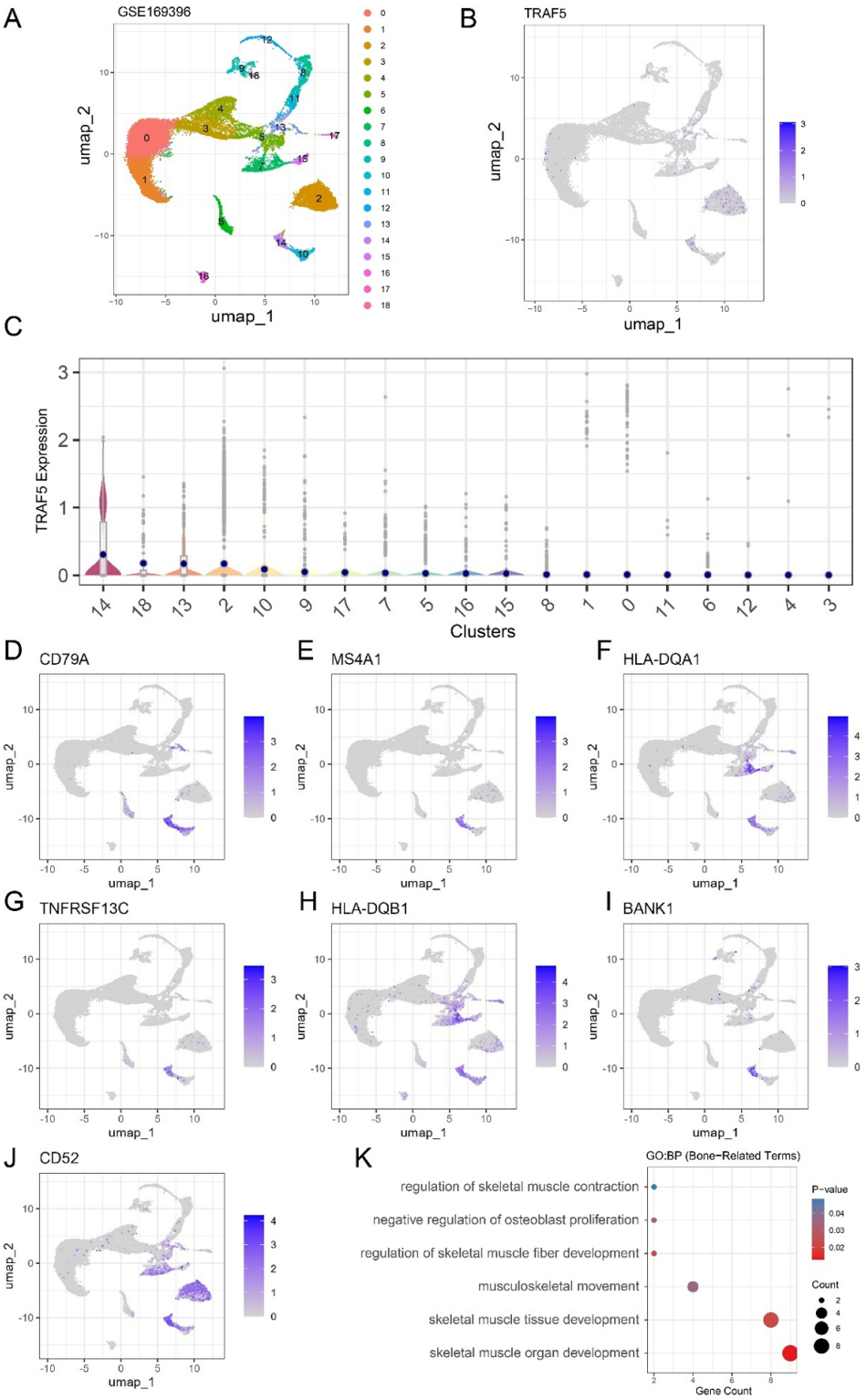


Fig. 2. Single-cell expression landscape of TRAF5 in human femoral-head tissue. (A) Uniform manifold approximation and projection (UMAP) clustering of cells in GSE169396. Cell-type annotations for clusters 0–18 are provided in **Supplementary Table 1**. (B) Distribution of TRAF5 expression across cell clusters. (C) Violin plot of TRAF5 expression by cluster. (D–J) UMAP feature plots of marker genes used to characterize cluster 14. (K) Gene Ontology biological-process enrichment analysis for cluster 14.

4A,B). This was accompanied by an increased abundance, size, and nuclearity of TRAP-positive multinucleated cells (Fig. 4C). Conversely, short hairpin RNA-mediated knockdown of TRAF5 was shown to reduce TRAF5 mRNA expression (Fig. 4D), TRAF5 protein expression (Fig. 4E), and the formation of mature multinucleated osteoclasts

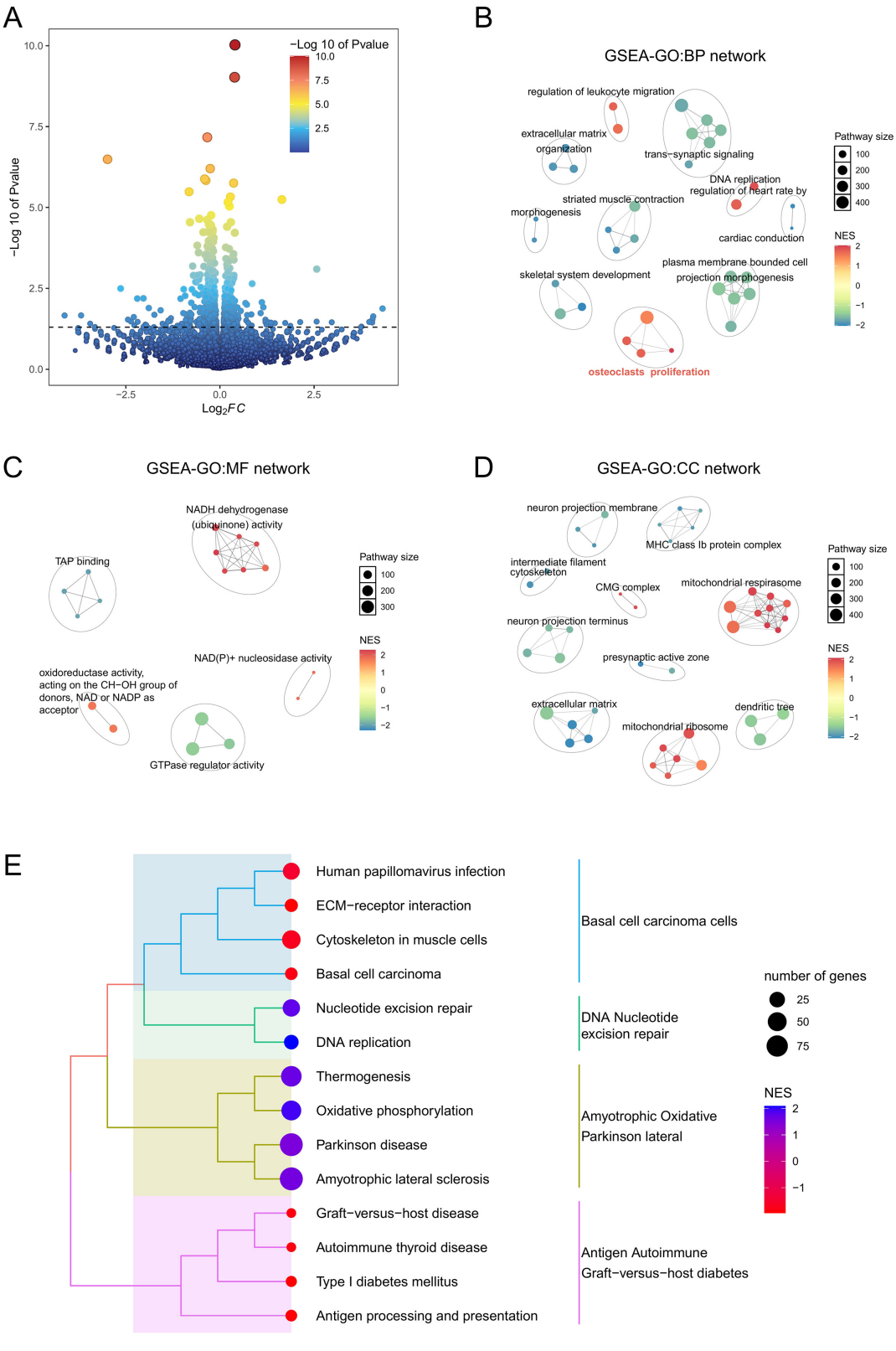


Fig. 3. Transcriptomic changes associated with TRAF5 overexpression in RAW264.7 cells. (A) Volcano plot of differentially expressed genes. (B–D) Gene set enrichment analysis networks for biological process, molecular function, and cellular component. Node size denotes pathway size, while color denotes normalized enrichment score. (E) Hierarchical clustering of enriched pathways. Bubble size denotes gene count, while color denotes normalized enrichment score.

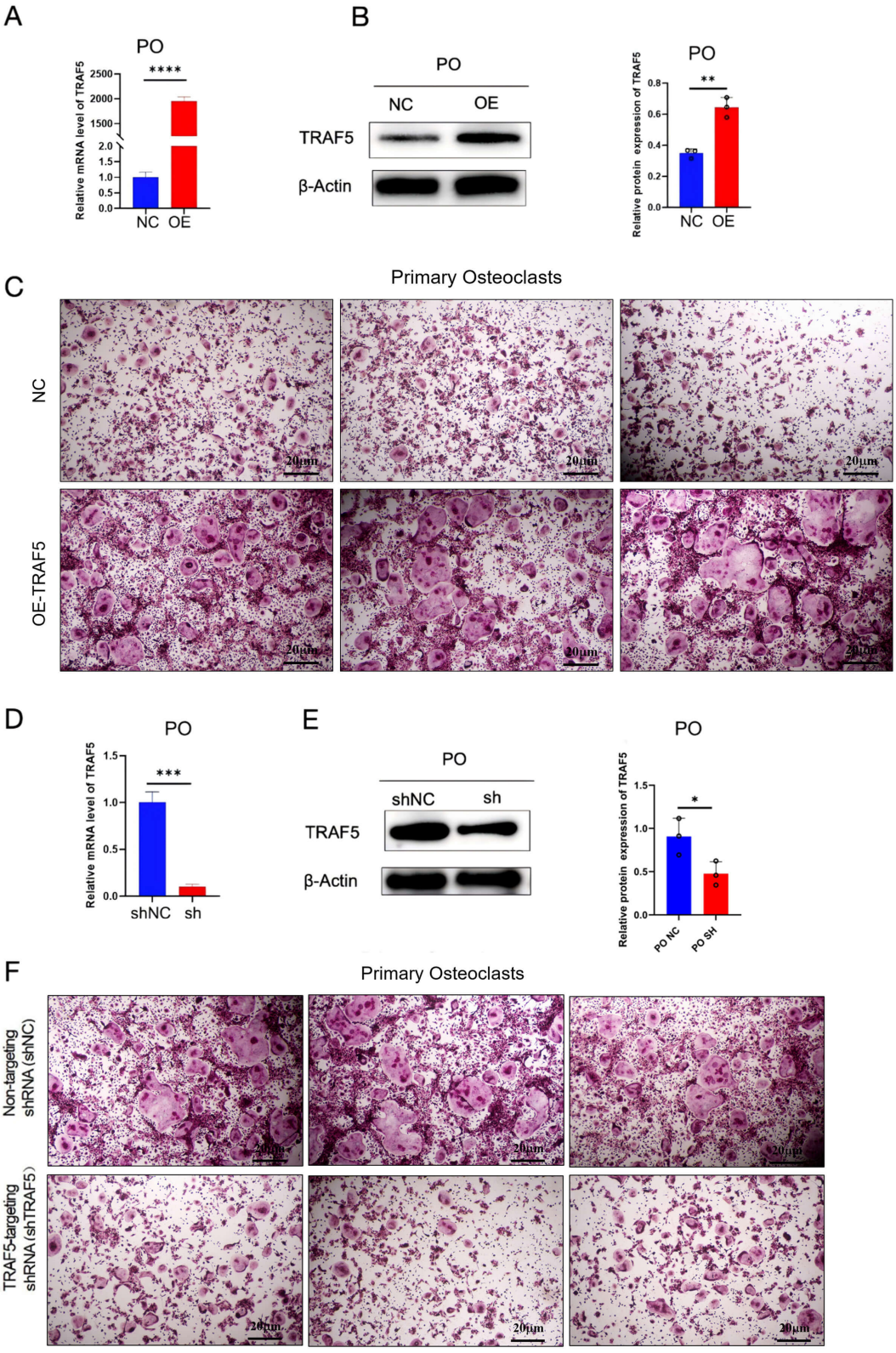


Fig. 4. TRAF5 promotes osteoclast formation in primary cultures. (A,B) RT-qPCR and Western blot analyses confirm TRAF5 overexpression. (C) Representative TRAP staining in negative-control and TRAF5-overexpression groups (Scale bar = 20 μm). (D,E) RT-qPCR and Western blot analyses of TRAF5 expression after shRNA treatment. (F) Representative TRAP staining after control or TRAF5-targeting short hairpin RNA treatment. *$p < 0.05$, **$p < 0.01$, ***$p < 0.001$, ****$p < 0.0001$; Scale bar = 20 μm. RT-qPCR, reverse transcription quantitative polymerase chain reaction.

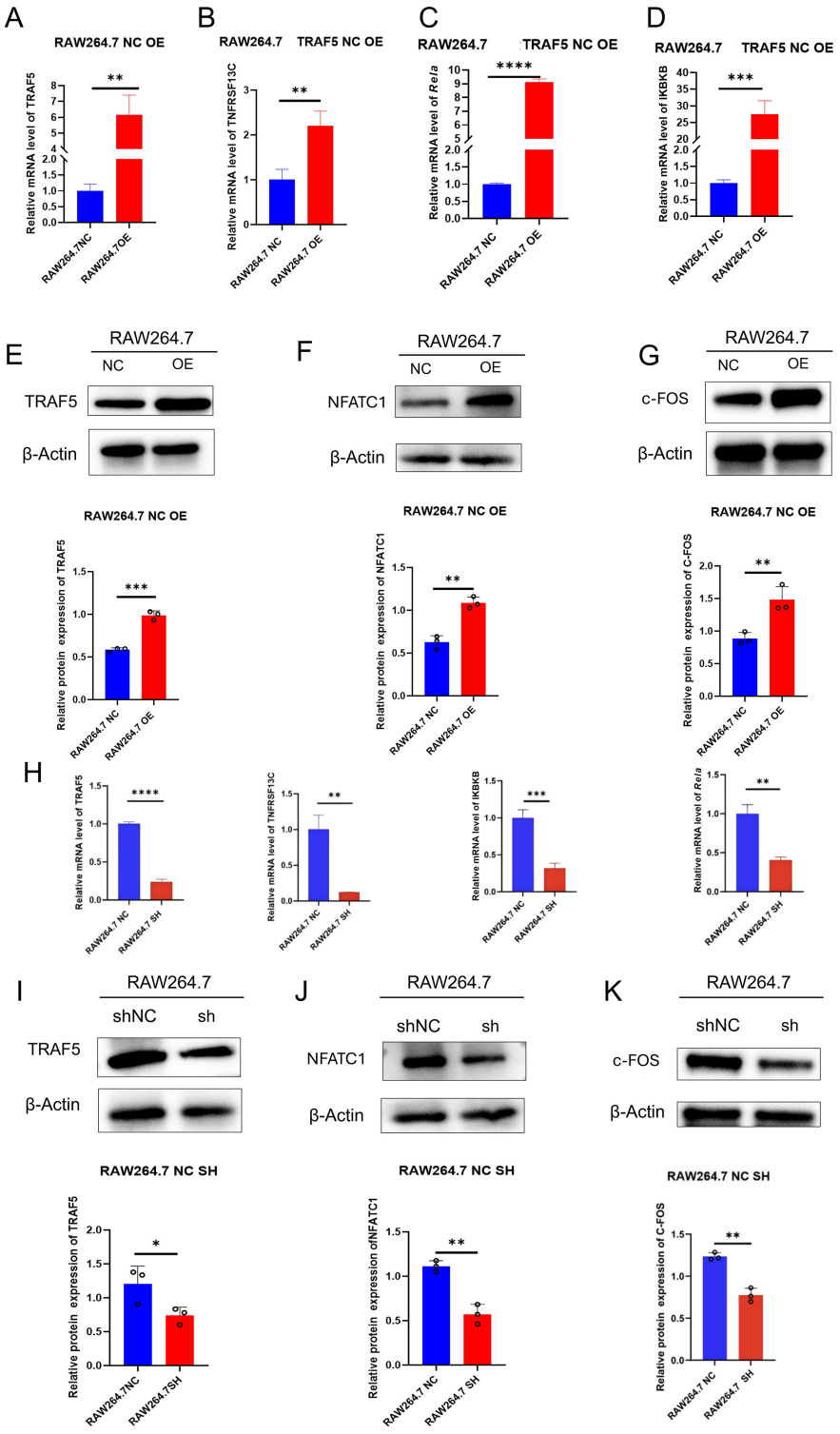


Fig. 5. TRAF5 alters osteoclastogenic signaling-related expression in RAW264.7 cells. (A–D) RT-qPCR analysis of TRAF5, TNFRSF13C, *Rela*, and IKBKB transcripts following TRAF5 overexpression. (E–G) Western blot and densitometric analyses of TRAF5, NFATc1, and c-FOS after TRAF5 overexpression. (H) RT-qPCR analysis of TRAF5, TNFRSF13C, IKBKB, and *Rela* transcripts after TRAF5 knockdown. (I–K) Western blot and densitometric analyses of TRAF5, NFATc1, and c-FOS after TRAF5 knockdown. Data are presented as the mean ± SD. IKBKB, inhibitor of nuclear factor kappa B kinase subunit beta; the RT-qPCR measurements represent IKBKB mRNA expression. *$p < 0.05$, **$p < 0.01$, ***$p < 0.001$, ****$p < 0.0001$. c-FOS, Fos proto-oncogene, AP-1 transcription factor subunit; SD, standard deviation.

(Fig. 4F). These gain- and loss-of-function results support a pro-osteoclastogenic role for TRAF5 under the experimental conditions.

3.5 TRAF5 Alters the Expression of TNFRSF13C, IKBKB/Rela, c-FOS, and NFATc1

TRAF5 overexpression in RAW264.7 cells increased TRAF5 mRNA and protein levels (Fig. 5A,E), TNFRSF13C, IKBKB, and *Rela* transcript levels (Fig. 5B–D), and c-FOS and NFATc1 protein levels (Fig. 5F,G). TRAF5 knockdown reduced TRAF5 and TNFRSF13C transcripts, NFATc1 protein expression (Fig. 5H–J), and c-FOS protein expression (Fig. 5K). These expression changes are consistent with the engagement of an IKBKB/*Rela*-related osteoclastogenic program. Because phosphorylation, nuclear translocation, DNA binding, and reporter activity were not measured, the experiments do not directly establish activation of NF-κB.

3.6 TNFRSF13C Silencing Attenuates TRAF5-Associated Osteoclastogenic Responses

In primary osteoclast cultures, TRAF5 overexpression increased c-FOS and NFATc1 protein levels, whereas TRAF5 knockdown reduced c-FOS levels, with a nonsignificant decrease in NFATc1 (Fig. 6A,B). In RAW264.7 cells, TNFRSF13C silencing reduced TRAF5 and TNFRSF13C mRNA levels and TRAF5 and NFATc1 protein levels (Fig. 6C,F,H), whereas TNFRSF13C and c-FOS protein levels decreased without statistical significance (Fig. 6D,E). TNFRSF13C protein levels showed a nonsignificant increase after TRAF5 overexpression but decreased after TRAF5 knockdown (Fig. 6G).

In rescue experiments, TNFRSF13C silencing attenuated the increases in c-FOS and NFATc1 associated with TRAF5 overexpression (Fig. 6I,J). In primary osteoclast cultures, TNFRSF13C silencing significantly reduced the mRNA levels of TNFRSF13C, IKBKB, and *Rela* (Fig. 6K). In primary osteoclast cultures, TNFRSF13C silencing significantly reduced the TRAF5 overexpression-induced increase in TRAP-positive multinucleated cells (Fig. 6L,M). These findings support the functional involvement of TNFRSF13C in TRAF5-associated osteoclastogenic responses in the tested models, although the direction and molecular basis of their regulation require further study.

3.7 Local TRAF5-Targeting shRNA Treatment is Associated With Attenuated Titanium Particle-Induced Calvarial Osteolysis

Treatment with titanium particles resulted in calvarial thinning and erosion, inflammatory soft-tissue infiltration, and accumulation of TRAP-positive osteoclasts compared with controls (Fig. 7A,B). Micro-computed tomography showed reduced BV/TV and increased total porosity after particle treatment (Fig. 7C,D,F,G). Local administration of TRAF5 short hairpin RNA lentivirus was associated with higher BV/TV and lower porosity compared with the titanium particle-only group, as assessed by micro-computed tomography (Fig. 7E–G). These *in vivo* findings suggest a possible contribution of TRAF5 to particle-induced bone loss in the local calvarial model.

In an independent validation cohort, treatment with titanium particles increased calvarial TRAF5, TNFRSF13C, and *Rela* mRNA expression relative to controls, whereas TRAF5-targeting shRNA lentivirus reduced the expression of all three genes relative to the titanium particle-only group (Fig. 8). These findings provide transcript-level evidence of local TRAF5 suppression. Local TRAF5 protein expression was not assessed. These *in vivo* findings should be interpreted with caution because the experiment included only three mice per group and lacked a titanium particle plus non-targeting shRNA lentivirus control group.

4. Discussion

This study combined public transcriptomic analyses, computational structural modeling, cellular gain- and loss-of-function experiments, and a murine calvarial model to examine TRAF5 in wear particle-induced osteolysis. The main findings were that TRAF5 was prioritized as a titanium particle-responsive RANK-associated candidate; TRAF5 and TNFRSF13C were detected in a predominantly B-cell-associated single-cell cluster; TRAF5 manipulation altered osteoclast formation and c-FOS/NFATc1 expression; TNFRSF13C silencing attenuated TRAF5-associated responses; and local TRAF5-targeting shRNA treatment was associated with reduced titanium particle-induced calvarial bone loss. Together, these results support a role for TRAF5 in wear particle-associated osteoclastogenesis, and also suggest the functional involvement of TNFRSF13C in this process.

Aseptic loosening develops within a chronic inflammatory microenvironment in which osteoclast-mediated bone resorption exceeds bone formation [25]. RANKL/RANK signaling is central to osteoclast differentiation [26,27], but the relative contributions of receptor-associated adaptors in the wear particle microenvironment remain incompletely defined. The broad transcriptional response observed in the GSE234863 dataset is consistent with previous evidence that titanium particles engage inflammatory and osteolytic pathways [28]. Although whole-tissue transcriptomic profiles may reflect both intracellular changes and shifts in cellular composition, their integration with subsequent cellular experiments allowed TRAF5 to be prioritized for functional validation.

TRAF6 is the canonical RANK adaptor, whereas TRAF5 has been reported to contribute to RANKL- and tumor necrosis factor-α-induced osteoclastogenesis [18,29]. Our intersection analysis prioritized TRAF5 in the titanium particle context, while the cellular experiments supported a pro-osteoclastogenic effect. Furthermore, AlphaFold3 generated a structurally compatible RANK-TRAF5 model, providing a testable structural hypothesis that complements

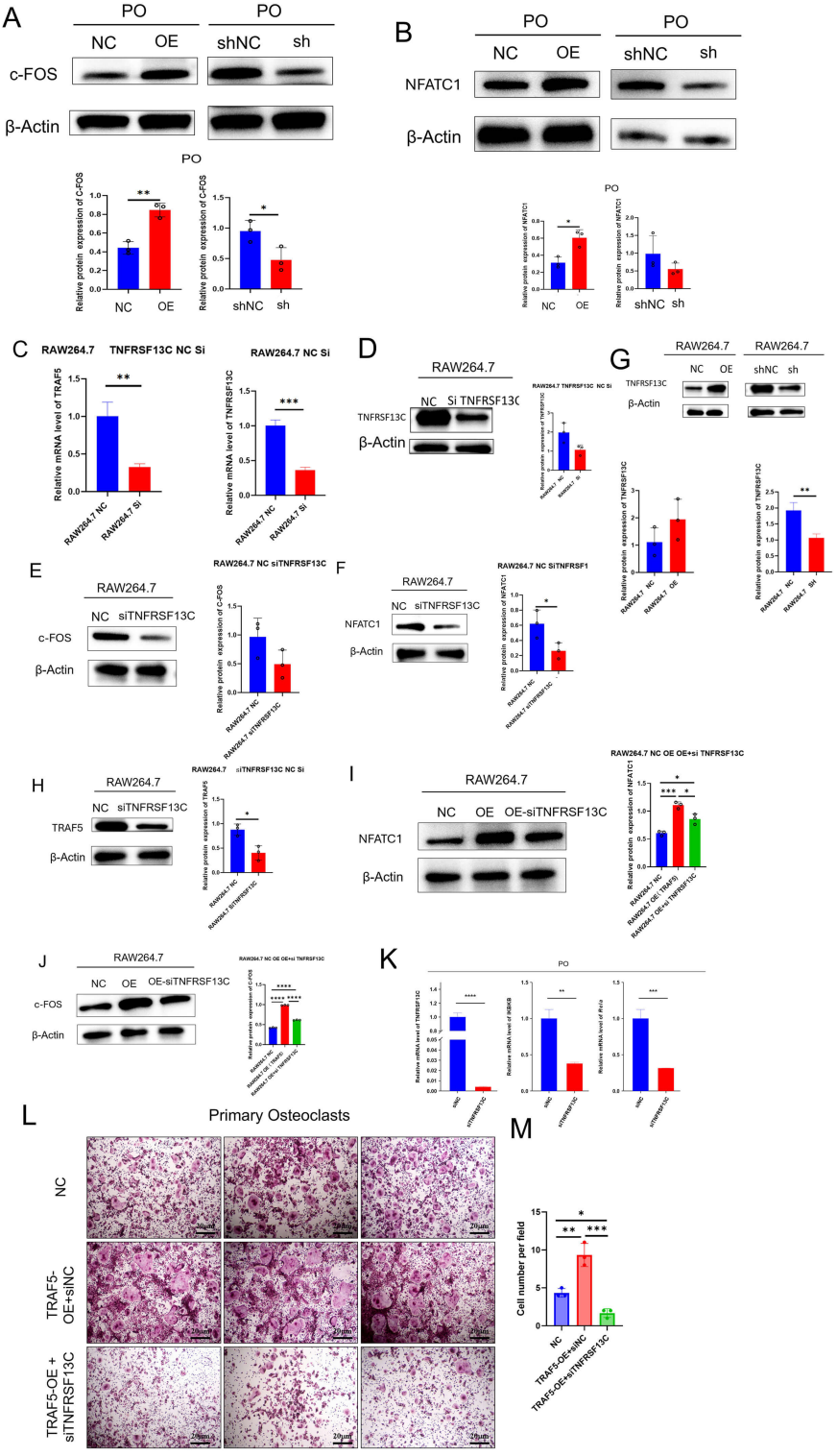


Fig. 6. TNFRSF13C silencing attenuates TRAF5-associated osteoclastogenic responses. (A,B) Western blot analysis of c-FOS and NFATc1 after TRAF5 overexpression or knockdown in primary osteoclast cultures. (C,D) TRAF5 and TNFRSF13C expression after TNFRSF13C silencing in RAW264.7 cells. (E,F) c-FOS and NFATc1 expression after TNFRSF13C silencing. (G) TNFRSF13C expression after TRAF5 overexpression or knockdown. (H) TRAF5 expression after TNFRSF13C silencing. (I,J) Rescue experiments evaluating c-FOS and NFATc1 after TRAF5 overexpression with or without TNFRSF13C silencing. (K) RT-qPCR analysis of TNFRSF13C, IKBKB, and *Rela* mRNA expression in primary osteoclast cultures. (L) Representative TRAP staining in primary osteoclast cultures (Scale bar = 20 μm). (M) Quantification of TRAP-positive multinucleated cells. IKBKB, inhibitor of nuclear factor kappa B kinase subunit beta; the RT-qPCR measurements represent IKBKB mRNA expression. *$p < 0.05$, **$p < 0.01$, ***$p < 0.001$, ****$p < 0.0001$.

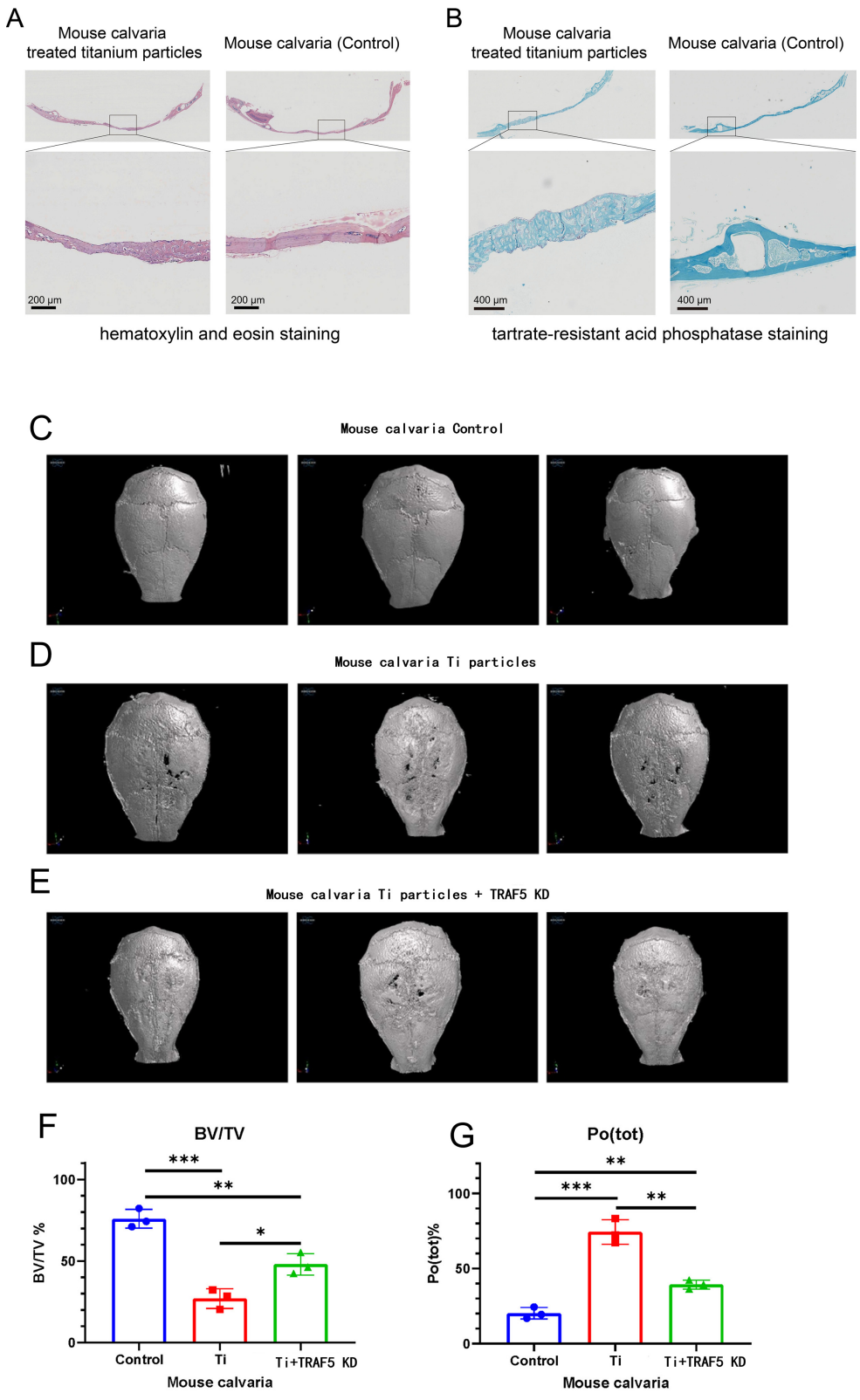


Fig. 7. Local TRAF5 silencing attenuates titanium particle-induced calvarial osteolysis. (A) Representative hematoxylin and eosin-stained calvarial sections (Scale bar = 200 μm). (B) Representative TRAP-stained sections (Scale bar = 400 μm). (C–E) Representative micro-computed tomography reconstructions of control, titanium particle-treated, and titanium particle plus TRAF5-targeting shRNA lentivirus groups. (F,G) Quantification of bone volume fraction (BV/TV) and total porosity. *$p < 0.05$, **$p < 0.01$, ***$p < 0.001$.

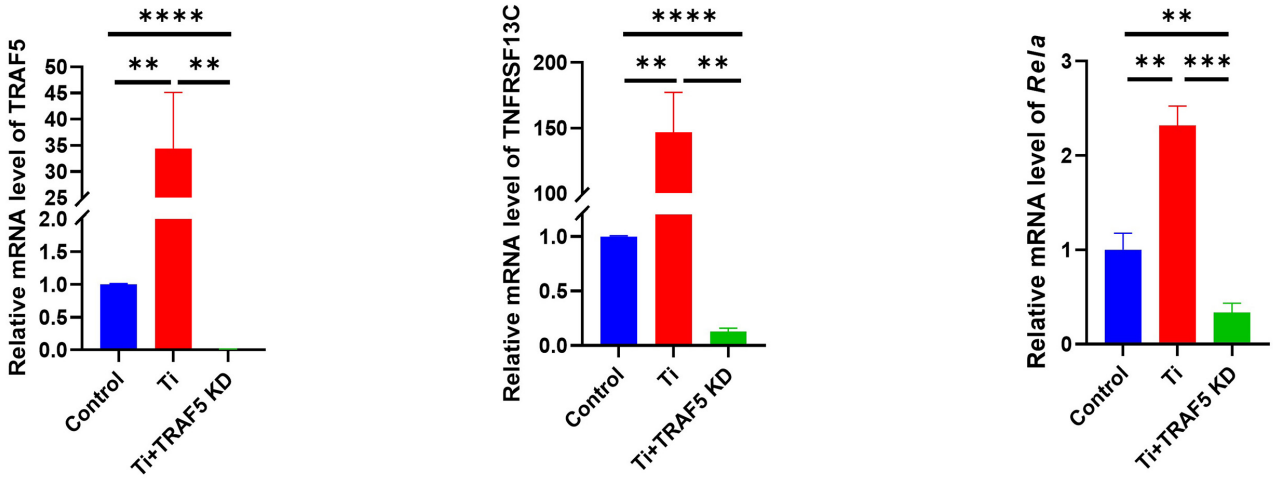


Fig. 8. Relative mRNA expression of TRAF5, TNFRSF13C, and *Rela* in mouse calvarial tissues. RT-qPCR analysis of calvarial tissues from the control, titanium particle (Ti), and Ti plus TRAF5-targeting shRNA lentivirus (Ti+TRAF5 KD) groups. Data are presented as the mean ± SD (n = 3 mice per group). $^{**}p < 0.01$, $^{***}p < 0.001$, $^{****}p < 0.0001$.

the transcriptomic and functional findings. Direct interaction will require confirmation by biochemical or cell-based assays.

TRAF5 overexpression was associated with transcriptional programs related to mitochondrial respiration and oxidative phosphorylation. Because osteoclast differentiation, fusion, and bone resorption require substantial metabolic adaptation [30], these findings suggest that TRAF5-associated osteoclastogenesis may be accompanied by coordinated metabolic remodeling. Functional metabolic studies will be required to determine whether this transcriptional signature is necessary for the pro-osteoclastogenic effects of TRAF5.

The expression changes involving TRAF5 and TNFRSF13C, together with the rescue experiments, support the functional involvement of TNFRSF13C in TRAF5-associated osteoclastogenic responses, including c-FOS and NFATc1 expression and osteoclast formation. These findings extend the known biology of TNFRSF13C beyond its established role in B-cell signaling and suggest that it may also be involved in osteoclastogenic regulation. In a related study [31], artesunate reduced bone loss and inflammation in ovariectomized rats, accompanied by decreased NF-κB p65 and Notch1 expression, further highlighting the potential involvement of these signaling pathways in bone remodeling. Although the expression patterns are consistent with NF-κB-related signaling, direct pathway-activation studies are required to define the precise mechanism.

Local administration of TRAF5-targeting shRNA lentivirus was associated with reduced bone loss and porosity in the calvarial model, providing preliminary *in vivo* support for the cellular findings. In an independent validation cohort, the expression of calvarial TRAF5 mRNA was lower after TRAF5-targeting shRNA lentivirus treatment than after treatment with titanium particles alone, with concomitant reductions in TNFRSF13C and *Rela* mRNA expression. These results provide additional transcript-level support for local TRAF5 targeting. However, because the calvarial model does not reproduce implant loading or joint anatomy, further validation in cell-specific and implant-bearing models is needed to establish its relevance to periprosthetic disease.

5. Limitations

Several limitations of this study should be acknowledged. First, the public transcriptomic datasets were derived from heterogeneous tissue sources, and the single-cell dataset was not generated from a titanium particle model. Second, the proposed molecular relationships are supported mainly by association analyses, expression changes, and rescue experiments, but have not been validated by direct protein interaction or NF-κB pathway activation assays. In addition, some of the protein expression comparisons shown in Fig. 6 were limited by small sample sizes and require validation in larger samples. Only titanium particles were examined in this study, and therefore it is uncertain whether the observed TRAF5-associated responses extend to other types of wear particles. Third, the oxidative phosphorylation-related findings were based on transcriptomic enrichment rather than functional metabolic assays. Finally, the *in vivo* experiments included only three mice per group, and the calvarial model does not recapitulate implant loading or joint anatomy. The absence of a TiPs plus non-targeting shRNA lentivirus control group precludes the exclusion of nonspecific effects arising from the lentiviral vector or local injection procedure. Although reduced calvarial TRAF5 mRNA expression was observed in an independent validation cohort, local TRAF5 knockdown was not verified at the protein level. To further clarify

the underlying mechanisms and validate the current findings, future studies should employ direct interaction and pathway-activation assays, together with TRAF5-knockout or osteoclast-specific genetic models and implant-bearing osteolysis models.

6. Conclusions

These findings support a positive regulatory role for TRAF5 in osteoclast differentiation. TRAF5 and TNFRSF13C showed a bidirectional association at the expression level. Moreover, TNFRSF13C silencing attenuated TRAF5 overexpression-associated increases in c-FOS/NFATc1 expression and osteoclast formation, suggesting it is functionally involved in the pro-osteoclastogenic effects of TRAF5. Exploratory *in vivo* findings showed that local administration of TRAF5-targeting shRNA lentivirus resulted in attenuation of titanium particle-induced calvarial osteolysis. Collectively, these findings suggest that TRAF5 contributes to osteoclastogenesis and titanium particle-induced osteolysis, and that its functional relationship with TNFRSF13C provides a basis for further mechanistic investigation and evaluation of the potential utility of targeting TRAF5-related signaling.

Abbreviations

BMDM, bone marrow-derived macrophage; BV/TV, bone volume/total volume; GEO, Gene Expression Omnibus; GSEA, gene set enrichment analysis; IKBKB, inhibitor of nuclear factor kappa B kinase subunit beta; NFATc1, nuclear factor of activated T cells 1; NF-κB, nuclear factor kappa B; PAE, predicted aligned error; PPI, protein-protein interaction; RANK, receptor activator of nuclear factor kappa B; RANKL, receptor activator of nuclear factor kappa B ligand; RNA-seq, RNA sequencing; RT-qPCR, reverse transcription quantitative polymerase chain reaction; scRNA-seq, single-cell RNA sequencing; TNFRSF13C, tumor necrosis factor receptor superfamily member 13C; TRAF5, tumor necrosis factor receptor-associated factor 5; TRAP, tartrate-resistant acid phosphatase.

Availability of Data and Materials

The GSE234863 and GSE169396 datasets analyzed in this study are publicly available through the Gene Expression Omnibus. The datasets used and analyzed during the current study are available from the corresponding author on reasonable request.

Author Contributions

HML: Conceptualization, Formal analysis, Writing - original draft. JHL: Data curation, Investigation, Writing - review and editing. HZ: Data curation, Investigation, Writing - review and editing. YYL: Conceptualization, Methodology, Supervision, Writing - review and editing. All authors contributed to editorial changes in the manuscript. All authors read and approved the final manuscript. All authors have participated sufficiently in the work and agreed to be accountable for all aspects of the work.

Ethics Approval and Consent to Participate

The animal study was reviewed and approved by the Institutional Animal Care and Use Committee of the Fourth Affiliated Hospital of Harbin Medical University (approval no. 2025-DWSYLLCZ-142). The animal procedures were conducted in accordance with the Guide for the Care and Use of Laboratory Animals (8th edition, National Research Council, 2011) and the ARRIVE guidelines.

Acknowledgment

Not applicable.

Funding

This work was supported by the Special Subsidized Research Program of the Fourth Affiliated Hospital of Harbin Medical University (HYDSYTB202229).

Conflicts of Interest

The authors declare no conflicts of interest.

Declaration of AI and AI-Assisted Technologies in the Writing Process

During the preparation of this manuscript, the authors used ChatGPT (OpenAI) to assist with language editing, manuscript refinement, and improvement of textual clarity. No AI tool was used to generate or analyze experimental data, create or modify scientific figures, or determine the scientific conclusions of the study. The authors reviewed and revised all AI-assisted content and take full responsibility for the accuracy and integrity of the final manuscript.

Supplementary Material

Supplementary Table 1 lists the cell-type annotations for clusters 0–18. Supplementary Table 2 lists the top 30 marker genes for each cluster. Supplementary material associated with this article can be found, in the online version, at https://doi.org/10.31083/FBL56630.

References

[1] Healy WL, Della Valle CJ, Iorio R, Berend KR, Cushner FD, Dalury DF, et al. Complications of total knee arthroplasty: standardized list and definitions of the Knee Society. Clinical Orthopaedics and Related Research. 2013; 471: 215–220. https://doi.org/10.1007/s11999-012-2489-y

[2] Yin J, Yin Z, Lai P, Liu X, Ma J. Pyroptosis in Periprosthetic Osteolysis. Biomolecules. 2022; 12: 1733. https://doi.org/10.3390/biom12121733

[3] Goodman SB, Pajarinen J, Yao Z, Lin T. Inflammation and Bone Repair: From Particle Disease to Tissue Regeneration. Frontiers in Bioengineering and Biotechnology. 2019; 7: 230. https://doi.org/10.3389/fbioe.2019.00230

[4] Terkawi MA, Matsumae G, Shimizu T, Takahashi D, Kadoya K, Iwasaki N. Interplay between Inflammation and Pathological Bone Resorption: Insights into Recent Mechanisms and Pathways in Related Diseases for Future Perspectives. International Journal of Molecular Sciences. 2022; 23: 1786. https://doi.org/10.3390/ijms23031786
[5] Yin L, Sun C, Zhang J, Li Y, Wang Y, Bai L, et al. Critical signaling pathways in osteoclast differentiation and bone resorption: mechanisms and therapeutic implications for periprosthetic osteolysis. Frontiers in Cell and Developmental Biology. 2025; 13: 1639430. https://doi.org/10.3389/fcell.2025.1639430
[6] Yao F, Bao Y, Meng Q, Chen Y, Zhao L, Wang P, et al. Periprosthetic osteolysis: Mechanisms and potential treatment strategies. Cellular Signalling. 2025; 131: 111758. https://doi.org/10.1016/j.cellsig.2025.111758
[7] Zhang G, Qin J, Xu W, Liu M, Wu R, Qin Y. Gene expression and immune infiltration analysis comparing lesioned and preserved subchondral bone in osteoarthritis. PeerJ. 2024; 12: e17417. https://doi.org/10.7717/peerj.17417
[8] Chen P, Guo HH, Wu L, Zhang S, Jin QH, Sun KN. The dual role of titanium particles in osteolysis: implications for gene therapy in prosthesis loosening. European Journal of Medical Research. 2025; 30: 216. https://doi.org/10.1186/s40001-025-02452-3
[9] Yoshida CA, Komori H, Maruyama Z, Miyazaki T, Kawasaki K, Furuichi T, et al. SP7 inhibits osteoblast differentiation at a late stage in mice. PloS One. 2012; 7: e32364. https://doi.org/10.1371/journal.pone.0032364
[10] Cai Y, Sun H, Song X, Zhao J, Xu D, Liu M. The Wnt/β-catenin signaling pathway inhibits osteoporosis by regulating the expression of TERT: an in vivo and in vitro study. Aging. 2023; 15: 11471–11488. https://doi.org/10.18632/aging.205136
[11] Hu L, Chen W, Qian A, Li YP. Wnt/β-catenin signaling components and mechanisms in bone formation, homeostasis, and disease. Bone Research. 2024; 12: 39. https://doi.org/10.1038/s41413-024-00342-8
[12] Ogawa T, Yokota S, Chen L, Ogawa Y, Nishida Y, Tokuhiro T, et al. Therapeutic Potential of Targeting Ferroptosis in Periprosthetic Osteolysis Induced by Ultra-High-Molecular-Weight Polyethylene Wear Debris. Biomedicines. 2025; 13: 170. https://doi.org/10.3390/biomedicines13010170
[13] Ma T, Liu Q, Zhang Z, Nan J, Liu G, Yang Y, et al. Fused exosomal targeted therapy in periprosthetic osteolysis through regulation of bone metabolic homeostasis. Bioactive Materials. 2025; 50: 171–188. https://doi.org/10.1016/j.bioactmat.2025.04.006
[14] Hikosaka-Kuniishi M, Iwata C, Ozawa Y, Ogawara S, Wakaizumi T, Itaya R, et al. The Role of TNF Receptor-Associated Factor 5 in the Formation of Germinal Centers by B Cells During the Primary Phase of the Immune Response in Mice. International Journal of Molecular Sciences. 2024; 25: 12331. https://doi.org/10.3390/ijms252212331
[15] Kim CM, Park HH. Comparison of Target Recognition by TRAF1 and TRAF2. International Journal of Molecular Sciences. 2020; 21: 2895. https://doi.org/10.3390/ijms21082895
[16] Guo Y, Xu Y, Xiong D, Zhou Y, Kang X, Meng C, et al. Molecular characterisation, expression and functional feature of TRAF6 in the King pigeon (Columba livia). Innate Immunity. 2020; 26: 490–504. https://doi.org/10.1177/1753425920920930
[17] Verma S, Sowdhamini R. Toll-like receptor 4 pathway evolutionary trajectory and functional emergence. Frontiers in Immunology. 2025; 15: 1494017. https://doi.org/10.3389/fimmu.2024.1494017
[18] Kanazawa K, Azuma Y, Nakano H, Kudo A. TRAF5 functions in both RANKL- and TNFalpha-induced osteoclastogenesis. Journal of Bone and Mineral Research: the Official Journal of the American Society for Bone and Mineral Research. 2003; 18: 443–450. https://doi.org/10.1359/jbmr.2003.18.3.443
[19] Chen Y, Chen M, Liu Y, Li Q, Xue Y, Liu L, et al. BAFF promotes follicular helper T cell development and germinal center formation through BR3 signal. JCI Insight. 2024; 9: e183400. https://doi.org/10.1172/jci.insight.183400
[20] Lim CS, Lee J, Kim JW, Lee JO. Highly ordered clustering of TNFα and BAFF ligand-receptor-intracellular adaptor complexes on a lipid membrane. Nature Communications. 2025; 16: 5551. https://doi.org/10.1038/s41467-025-61271-6
[21] Wang H, Mei D, Liang FQ, Xue ZY, Wang P, Liu RJ, et al. BAFF Promotes FLS Activation Through BAFFR-Mediated Non-canonical NF-κB Pathway and the Effects of CP-25. Inflammation. 2023; 46: 861–875. https://doi.org/10.1007/s10753-022-01774-2
[22] Wang M, Otto C, Fernández Zapata C, Dehlinger A, Gallaccio G, Diekmann LM, et al. Comprehensive analysis of B cell repopulation in ocrelizumab-treated patients with multiple sclerosis by mass cytometry and proteomics. IScience. 2025; 28: 112383. https://doi.org/10.1016/j.isci.2025.112383
[23] Lipsky PE, Vollenhoven RV, Dörner T, Werth VP, Merrill JT, Furie R, et al. Biological impact of iberdomide in patients with active systemic lupus erythematosus. Annals of the Rheumatic Diseases. 2022; 81: 1136–1142. https://doi.org/10.1136/annrheumdis-2022-222212
[24] Ntellas P, Dardiotis E, Sevdali E, Siokas V, Aloizou AM, Tsinti G, et al. TNFRSF13C/BAFFR P21R and H159Y polymorphisms in multiple sclerosis. Multiple Sclerosis and Related Disorders. 2020; 37: 101422. https://doi.org/10.1016/j.msard.2019.101422
[25] Drees P, Eckardt A, Gay RE, Gay S, Huber LC. Mechanisms of disease: Molecular insights into aseptic loosening of orthopedic implants. Nature Clinical Practice. Rheumatology. 2007; 3: 165–171. https://doi.org/10.1038/ncprheum0428
[26] Li B, Wang P, Jiao J, Wei H, Xu W, Zhou P. Roles of the RANKL-RANK Axis in Immunity-Implications for Pathogenesis and Treatment of Bone Metastasis. Frontiers in Immunology. 2022; 13: 824117. https://doi.org/10.3389/fimmu.2022.824117
[27] Blair HC, Soboloff J, Tourkova IL, McCall JL, Ray S, Rosenkranz ME, et al. Molecular regulation of bone turnover in juvenile idiopathic arthritis: animal models, cellular features and TNFα. Frontiers in Bioscience-Landmark. 2024; 29: 248. https://doi.org/10.31083/j.fbl2907248
[28] Fang G, Fu Y, Li S, Qiu J, Kuang M, Lin S, et al. The USP14-NLRC5 pathway inhibits titanium particle-induced osteolysis in mice by suppressing NF-κB and PI3K/AKT activities. The Journal of Biological Chemistry. 2020; 295: 7018–7032. https://doi.org/10.1074/jbc.RA119.012495
[29] Darnay BG, Besse A, Poblenz AT, Lamothe B, Jacoby JJ. TRAFs in RANK Signaling. In Wu H (ed.) Advances in Experimental Medicine and Biology (pp. 152–159). Springer New York: New York, NY. 2007. https://doi.org/10.1007/978-0-387-70630-6_12
[30] Abu-Amer Y. NF-κB signaling and bone resorption. Osteoporosis International: a Journal Established as Result of Cooperation between the European Foundation for Osteoporosis and the National Osteoporosis Foundation of the USA. 2013; 24: 2377–2386. https://doi.org/10.1007/s00198-013-2313-x
[31] Wang G, Tan J, Huang C, Xu Y, Yang Z, Huo L. Based on NF-κB and Notch1/Hes1 signaling pathways, the mechanism of artesunate on inflammation in osteoporosis in ovariectomized rats was investigated. Frontiers in Bioscience-Landmark. 2024; 29: 266. https://doi.org/10.31083/j.fbl2907266